Applied Mathematical Modelling 58 (2018) 111–127

Contents lists available at ScienceDirect

Applied Mathematical Modelling

journal homepage: www.elsevier.com/locate/apm

Sparsity-promoting distributed charging control for plug-in electric vehicles over distribution networks☆,☆☆

Jueyou Li[a], Chaojie Li[b], Zhiyou Wu[a], Xiangyu Wang[c], Kok Lay Teo[d], Changzhi Wu[c,*]

[a] School of Mathematical Sciences, Chongqing Normal University, Chongqing, 400047, China
[b] School of Engineering, RMIT University, VIC 3000, Australia
[c] Australasian Joint Research Centre for Building Information Modelling, School of Built Environment, Curtin University, Bentley, WA, 6102, Australia
[d] Department of Mathematics and Statistics, Curtin University, Bentley, WA, 6102, Australia

ARTICLE INFO

Article history:
Received 27 November 2016
Revised 17 October 2017
Accepted 24 October 2017
Available online 31 October 2017

Keywords:
Distributed charging control
Sparsity-promoting control
ADMM
Plug-in electric vehicles
Feeder overload control

ABSTRACT

Uncoordinated charging of plug-in electric vehicles brings a new challenge on the operation of a power system as it causes power flow fluctuations and even unacceptable load peaks. To ensure the stability of power network, plug-in charging needs to be scheduled against the base load properly. In this paper, we propose a sparsity-promoting charging control model to address this issue. In the model, the satisfaction of customers is improved through sparsity-promoting charging where the numbers of charging time slots are optimized. Dynamic feeder overload constraints are imposed in the model to avoid any unacceptable load peaks, and thus ensure the network stability. Then, a distributed solution strategy is developed to solve the problem based on the alternating direction method of multipliers (ADMM) since most of power networks are managed typically in a distributed manner. During solving process, Lagrangian duality is used to transform the original problem into an equivalent dual problem, which can be decomposed into a set of homogeneous small-scaled sub-problems. Particularly, each sub-problem either has a closed-form solution or can be solved locally by an accelerated dual gradient method. The global convergence of the proposed algorithm is also established. Finally, numerical simulations are presented to illustrate our proposed method. In contrast to traditional charging models, our sparsity-promoting charging model not only ensures the stability of power network, but also improves the satisfaction of customers.

1. Introduction

To mitigate oil dependency and relieve greenhouse gas emissions, plug-in electric vehicles (PEVs) have been received wide public attentions [1,2]. PEVs are not only able to integrate renewable energy, reduce economic costs for PEV owners

☆ This research was partially supported by the NSFC 11501070, 11471062 and 61473326, by the Natural Science Foundation Projection of Chongqing cstc2015jcyjA00011 and cstc2017jcyjAX0253, and by the Key Laboratory of Optimization and Control, Ministry of Education, China.
☆☆ This article belongs to the Special Issue: The 10th International Conference on Optimization and Control with Application.
* Corresponding author.
E-mail addresses: lijueyou@cqnu.edu.cn (J. Li), chaojie.li@rmit.edu.au (C. Li), zywu@cqnu.edu.cn (Z. Wu), xiangyu.wang@curtin.edu.au (X. Wang), k.l.teo@curtin.edu.au (K.L. Teo), c.wu@curtin.edu.au (C. Wu).

https://doi.org/10.1016/j.apm.2017.10.034
0307-904X/

and energy providers, but also enhance energy infrastructure resilience if charging is managed properly [3–5]. In addition, it is possible for the PEV aggregator that has control over a fleet of PEVs to provide ancillary services by modulating the charging rate in the framework of a vehicle-to-grid (V2G) [6,7]. However, as the scale of PEV adoption grows, the focus on managing large population PEV resources while ensuring (i) the stability and capacity limits of power system, (ii) the satisfaction of PEV consumers, and (iii) the computational tractability and scalability, will become increasingly challengeable [1].

There is a growing body of studies on addressing optimal PEV population charging. Among them, two main catalogues of control architectures, centralized and decentralized, are extensively investigated in literature. Centralized charging control, e.g., [8,9] leverages a central controller to collect all the PEVs' information, and then communicates data between the controller and PEV users in order to compute the optimal load profile of the fleet. The challenge for a centralized charging method, is its scalability with respect to privacy, communication and computation [10].

With the advancement of metering infrastructures, decentralized charging control has attracted significant research attention since it not only alleviates the communication and computation burden but also is suitable for large-scale implementation in a parallel/distributed way [11,12]. In contrast to centralized charging control, decentralized charging scheme can offer better privacy protection for individual PEV consumers [10,13].

A wide range of decentralized algorithms have been developed in the literatures. In [11], Gan et al. designed a decentralized protocol and proposed an iterative algorithm to fill the night valleys optimally in electric loads. The operation of PEVs under balanced network constraints was tackled based on a water-filling algorithm [14]. In [12,13], the authors developed noncooperative game-theoretic schemes for obtaining a Nash Equilibrium in the large-scale regime. In [15], Tushar et al. investigated a hierarchical game model using the Stackelberg game between the utility (leader) and PEV users (followers). Based on the popular alternating direction method of multipliers (ADMM) method [16–22], Tan et al. in [23] designed a distributed algorithm for solving a demand response management model that integrates PEVs and distributed renewable generators. The work in [24] developed a comprehensive model for the electric vehicle aggregator to achieve the computational scalability by utilizing ADMM.

However, most of previous works for PEV smart charging primarily focused on the minimization of the total load variance or the overall charging cost of all PEVs over the distribution grid subjected to individual PEV constraints. Until recently, there are a lot of articles, which determine optimal PEV charging profiles by considering transformer and feeder overloads, refer to the literature review [25]. The work in [26] evaluated the impact of PEV loading on distribution system and summarized partial results of the impact of PEVs on one utility distribution feeder. In [27], Hilshey et al. analyzed the impact of PEV charging on overhead distribution transformers, and then proposed a novel smart charging algorithm that manages PEV charging based on estimated transformer temperatures. Considering the transformer aging risk, a data-driven charging strategy of PEV charging was proposed in [28]. The authors in [29] pointed out that uncontrolled and time-of-use charging profiles are the two strategies with the most negative impacts on the distribution transformers. They proposed a method to prevent transformers from overloading, while achieving a desirable level of valley filling at the grid level simultaneously. The impact of PEV loading on a residential distribution grid was analyzed in terms of power losses and voltage deviations [30]. The authors in [31] proposed a demand response strategy as a load shaping technique to improve the utilization of distribution transformers, and prevent it from overloading. Ghavami et al. in [32] pointed out that under certain scenarios, the feeder overloads may endanger the whole power grid, then they developed feeder overload control schemes in a reasonable topology structure of distribution network, also see [33]. The computational complexity is high since a large number of iterations are required to ensure the convergence of their proposed methods which is impractical to coordinate the charging for large-scale PEVs in practice. By considering the capacity constraints of the transmission lines, Ardakanian et al. [34] proposed a proportionally fair rate allocation strategy for charging each PEV. However, the total load of each PEV has not been taken into account and only static charging was considered.

Charging behavior can affect key battery characteristics, such as the state of health, the cycle life and the resistance impedance growth [35,36]. Intermittent charging will shorten the battery lifespan [11]. Therefore, how to decrease the number of charging to maintain battery health is important. On the other hand, a long waiting time to complete a charging task or/and frequent interruptions in the process of charging is unacceptable [37]. Both of them potentially make PEV owners discomfort. The recent work [38] shown that consumers' satisfaction is usually characterized by the sparsity of optimal solutions through sparse optimization technique, also see [39,40]. It is required that the solution of charging schedules should be sparse enough, which potentially mirrors users' satisfaction level as a sparse schedule means less frequency of charging. Of course, the minimal number of charging can be explicitly modeled by certain constraints, such as minimal on/off time [41]. However, if binary variables are introduced to formulate the problem, it will increase the computational complexity of the resulting model significantly.

This paper proposes a sparsity-promoting PEV charging control (SPCC) model, which can be implemented in a distributed manner. The major contributions of the paper are twofold:

(1) A sparsity-promoting model is proposed with dynamical feeder overload constraints to ensure the stability of the power network. The model minimizes the overall load variance while enhancing the accumulated satisfaction of all the PEV users subject to the limits on the feeder overload of power network. To the best of our knowledge, this is the first paper aiming at improving PEV users' comfort meanwhile considering the stability of the distribution network. As demonstrated through numerical examples, users' satisfaction can be enhanced by reducing the numbers of charging

Table 1
Nomenclature.

$\mathcal{N}$	Set of PEVs with $\mathcal{N}=\{1,\ldots,N\}$
$\mathcal{T}$	Set of discrete time slots with $\mathcal{T}=\{1,\ldots,T\}$
$\mathcal{L}$	Set of feeders with $\mathcal{L}=\{1,\ldots,L\}$
$x_{n,t}$	Charging rate of PEV n at time t
$e_{n,t}$	Discharging rate of PEV n at time t when driving
$S_{n,t}$	State of charge (SOC) of PEV n at time t
$S_n^{\min/\max}$	Minimum/maximum SOC values of PEV n allowed
B_n	Battery capacity of PEV n
d_t	Aggregated non-PEV demand at time t
$c_{l,t}$	Capacity of feeder l at time t for loading PEVs

time slots, owing to the sparsity-promoting scheme. Moreover, the security of the distribution power network can be ensured by the overload control on the feeders.

(2) A distributed method (see, Algorithm 2) based on the framework of ADMM is proposed to solve the proposed model. The main idea behind is to decouple the coupling constraints and decompose the original model into a set of small-scaled sub-problems, in which these sub-problems either enjoy a closed-form solution or can be solved locally by our proposed accelerated dual gradient method (see, Algorithm 1). The proposed strategy presented in Algorithm 2 is implemented in a fully distributed manner and scalable to solve other PEV charging control models. Moreover, the global convergence of the proposed Algorithm 2 is established theoretically and the explicit convergence rate of Algorithm 1 is obtained.

The remaining of this paper is organized as follows. We describe the system model and formulate the SPCC model in Section 2. In Section 3, we propose a distributed charging control algorithm (Algorithm 2) to solve the SPCC model and an accelerated dual gradient algorithm to solve the corresponding sub-problems (Algorithm 1), respectively. The convergence of the proposed algorithms is established through rigorously mathematical analysis (refer to Appendix). Simulations are conducted in Section 4. Finally, some conclusions and future works are given in Section 5.

1.1. Notation

Let $\mathbf{x}$ be a vector in $\mathbb{R}^p$, we use $||\mathbf{x}||_2$ to denote the standard Euclidean norm or ℓ_2-norm, i.e., $||\mathbf{x}||_2=\left(\sum_{i=1}^p x_i^2\right)^{1/2}$. We denote the ℓ_0-norm as a total number of non-zero elements in a vector $\mathbf{x}$, i.e., $||\mathbf{x}||_0=\#(i|x_i\neq 0)$. For a matrix $\mathbf{A}\in\mathbb{R}^{p\times q}$, we use $||\mathbf{A}||_F=(\sum_{i=1}^p\sum_{j=1}^q a_{ij}^2)^{1/2}$ to stand for the Frobenius norm of the matrix $\mathbf{A}$. Let $[\cdot]_+=\max\{0,\cdot\}$ be a positive projection operator.

2. System model

In this section, we establish a sparsity-promoting model to control PEV charging. We first model a system where an electric utility operates a finite set $\mathcal{N}$ of PEVs determining the charging schedule in a distribution network. Notations used are described in Table 1. Let $\mathbf{x}_n=(x_{n,1},\ldots,x_{n,T})^\top\in\mathbb{R}^T$ be the charging profile for PEV n across all the time slots and $\mathbf{x}=(\mathbf{x}_1,\ldots,\mathbf{x}_N)^\top\in\mathbb{R}^{N\times T}$ be the charging profile for all the PEVs in the network.

2.1. PEV charging constraints

Based on a piecewise linear model [12], the battery dynamics are described as below:

$$S_{n,t+1}=S_{n,t}+\frac{\varrho_n^+x_{n,t}}{B_n}\Delta t-\frac{e_{n,t}}{\varrho_n^-B_n}\Delta t, \tag{1}$$

$$S_n^{\min}\le S_{n,t}\le S_n^{\max}, \tag{2}$$

where $\varrho_n^+,\varrho_n^-\in(0,1]$ represent the energy conversion efficiencies of charging and discharging for PEV n, respectively. To prolong the lifespan of the batteries, it is recommended that the values $S_n^{\min}$ and $S_n^{\max}$ are 15%, and 90%, respectively [35]. Similarly to previous work [10], it can deduce the following constraints for the energy of PEV n from Eqs. (1) and (2),

$$\begin{aligned}\frac{B_n}{\varrho_n^+\Delta t}\left(S_n^{\min}-S_n^{\text{init}}\right)+\frac{\varrho_n^-}{\varrho_n^+}\sum_{\tau=1}^t e_{n,\tau}&\le\sum_{\tau=1}^t x_{n,\tau}\\&\le\frac{B_n}{\varrho_n^+\Delta t}\left(S_n^{\max}-S_n^{\text{init}}\right)+\frac{\varrho_n^-}{\varrho_n^+}\sum_{\tau=1}^t e_{n,\tau},\end{aligned} \tag{3}$$

where S_n^{init} is the initial SOC value of PEV n allowed.

Let $x_n^{\min}$ and $x_n^{\max}$ be the minimum and maximum charging power of PEV n, respectively, we have the following inequality constraints:

$$x_n^{\min} \le x_{n,t} \le x_n^{\max}, \ \ n \in \mathcal{N}, t \in \mathcal{T}. \tag{4}$$

The variable $x_{n,t}$ is non-zero if and only if PEV n is charged at time t. We denote $I_{n,t} = 1$ if PEV n is charged at time t; otherwise 0. Thus, the constraints below should be satisfied:

$$(1 - I_{n,t})x_{n,t} = 0, \ \ n \in \mathcal{N}, t \in \mathcal{T}. \tag{5}$$

In practice, we impose the following conservative constraint [10] that every PEV n reaches at least the final SOC value, S_n^{final}, at the end of the finite time horizon T,

$$\sum_{t=1}^{T} x_{n,t} \ge \frac{B_n}{Q_n^+ \Delta t}\left(S_n^{\text{final}} - S_n^{\text{init}}\right) + \frac{Q_n^-}{Q_n^+}\sum_{t=1}^{T} e_{n,t}. \tag{6}$$

For notational simplicity, define $\mathcal{X}_n^{(1)}$ as follows:

$$\mathcal{X}_n^{(1)} = \{\mathbf{x}_n \mid \mathbf{x}_n \text{ satisfies } (3)-(6)\}, \ \ n \in \mathcal{N}, \tag{7}$$

where the operational parameters $x_n^{\min/\max}$, $S_n^{\min/\max}$ and $S_n^{\text{init/final}}$ are assumed to be private for individual PEV user and pre-determined by external factors such as vehicle type and driving style. Note that the set $\mathcal{X}_n^{(1)}$ defined in (7) is a local constraint, which temporally couples the charging schedules across all the time slots for PEV user n. Let

$$\mathcal{X}^{(1)} = \mathcal{X}_1^{(1)} \times \cdots \times \mathcal{X}_n^{(1)} \times \cdots \times \mathcal{X}_N^{(1)} \tag{8}$$

be the accumulated constraints for all PEVs.

2.2. Feeder capacity constraints

The distribution network is modeled as a tree with the radial structure, which is rooted at the substation, e.g., see Fig. 1. All the PEVs are attached to leaf nodes of the tree. Let $\Pi_n \subseteq \mathcal{L}$ be the set of feeders that convert power from the substation to PEV n, and let $\Gamma_l = \{n : l \in \Pi_n\}$ be the set of PEVs that use the feeder l to transfer power.

Let $D_{l,t}$ be the base demand load transmitted via the feeder l at time t. We assume the feeder l at time t that can support the maximum PEV demand is $c_{l,t} = C_l - D_{l,t}$, where C_l is the maximum loading capacity of the feeder l. Thus, we have the following global constraints on the feeder capacity,

$$\sum_{n \in \Gamma_l} x_{n,t} \le c_{l,t}, \quad t \in \mathcal{T}, l \in \mathcal{L}, \tag{9}$$

which spatially couples the demand of those PEV consumers that make use of the feeder l at time t.

2.3. Sparsity-promoting of PEV charging control model

The utility seeks to minimize the variance of net load while improving the satisfaction of PEV users subject to the constraints of PEV charging and the feeder capacity limits of power network. This is modeled by the following optimization problem,

$$\begin{aligned} \min_{\mathbf{x} \in \mathcal{X}^{(1)}} \ & \sum_{t \in \mathcal{T}} \left(d_t + \sum_{n \in \mathcal{N}} x_{n,t} \right)^2 + \gamma \sum_{n \in \mathcal{N}} ||\mathbf{x}_n||_0 \\ \text{s.t.} \ & \sum_{n \in \Gamma_l} x_{n,t} \le c_{l,t}, \ \ t \in \mathcal{T}, l \in \mathcal{L}, \end{aligned} \tag{10}$$

where $\gamma > 0$ is a weighing parameter representing the trade-off between the variance of total load and the aggregated satisfaction of all the PEV users.

The first term in (10) stands for the variance of the total load curve, which has the potential to fill the valley of the demand load. The second term in (10) is the cardinality minimization of the charging schedule $\mathbf{x}_n$ for PEV user n, accounting for the comfort of PEV users to some extent [38]. On one hand, the users try to reduce the number of charging as many as possible for protecting battery health. On the other hand, PEV users would prefer to finish a task as quickly as possible as they want to minimize interruption or restarting PEVs charging. Waiting longer to complete a task is unacceptable to most of users. As a consequence, two objectives to measure the satisfaction of users can be unified by inducing a sparse charging schedule given by the second term of (10). Note that the second term of the model (10) introduced in this paper is motivated by the recent works [38,39].

The cardinality minimization $||\mathbf{x}_n||_0$ plays a significant role in modeling the sparsity of the solution. However, the minimization of $||\mathbf{x}_n||_0$ is still a computational challenge since $||\mathbf{x}_n||_0$ is a non-convex function and directly optimizing this function even over linear constraints is proved to be an NP-hard problem [16]. To circumvent the computational difficulty,

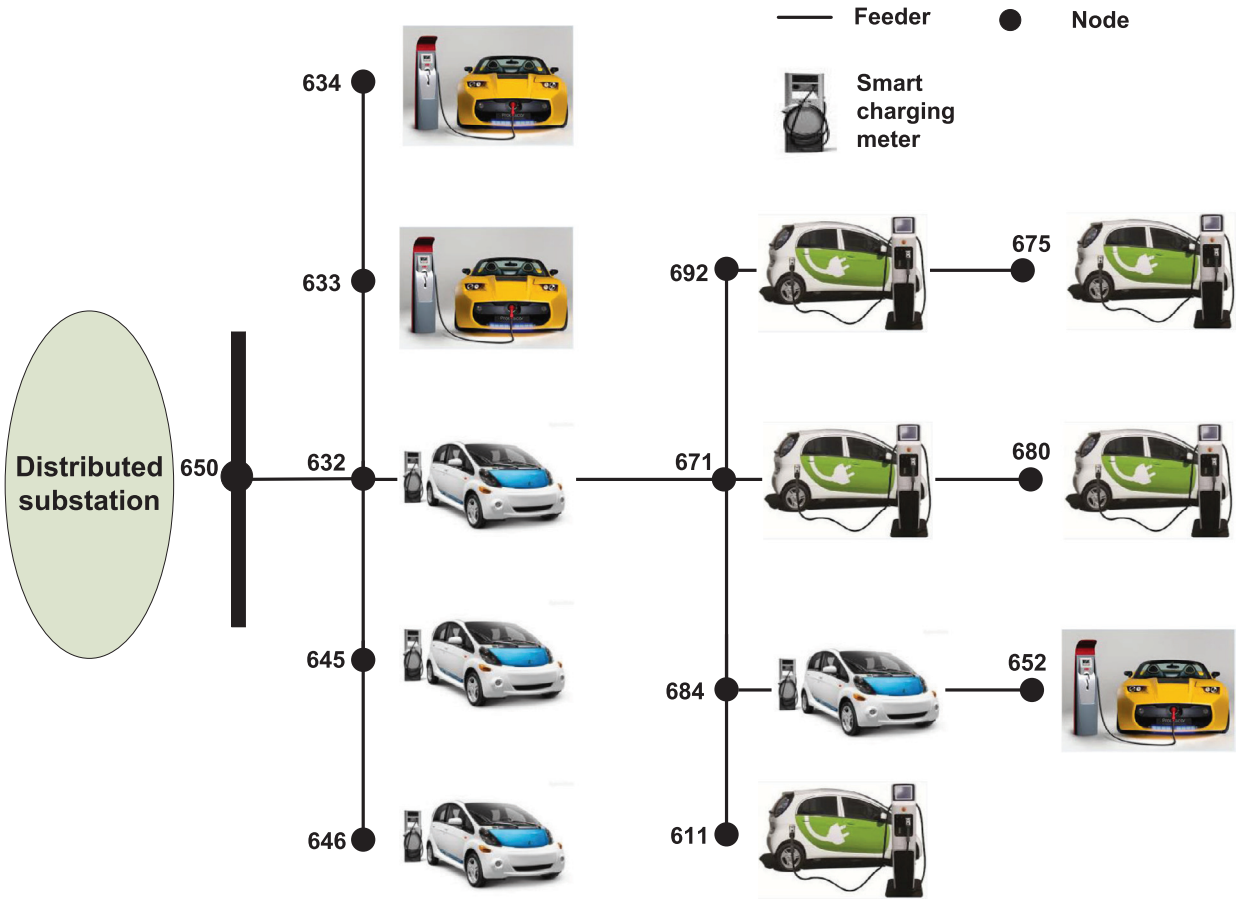

Fig. 1. Distribution network with radial structure for charging PEV.

we often approximate $||\mathbf{x}_n||_0$ by the tightest convex approximation $||\mathbf{x}_n||_1$. In fact, in many situations, the ℓ_1-minimization can recover exactly the sparse solution of ℓ_0-minimization [16,40]. This powerful sparse optimization technique seems to just start finding its applications in power system analysis. Dörfler et al. [39] employed a recently-introduced paradigm of sparsity-promoting optimal control to simultaneously identify the optimal control structure and optimized the closed-loop performance. Phan et al. [40] used the ℓ_1-norm to minimize the number of post-contingency corrections for security-constrained optimal power flow problems. The work [38] exploited a sparse load shifting strategy to enhance customers's comfort for scheduling residential smart appliances in demand side management.

Resorting to the ℓ_1 convex approximation, we remodel the problem (10) as the following sparsity-promoting charging control (SPCC) model,

$$\begin{aligned} \min_{\mathbf{x}\in\mathcal{X}^{(1)}} \quad & \left\{ G_\gamma(\mathbf{x}) := \sum_{t\in\mathcal{T}} (d_t + \sum_{n\in\mathcal{N}} x_{n,t})^2 + \gamma \sum_{n\in\mathcal{N}} ||\mathbf{x}_n||_1 \right\} \\ \text{s.t.} \quad & \sum_{n\in\Gamma_l} x_{n,t} \le c_{l,t}, \ \ t \in \mathcal{T}, l \in \mathcal{L}. \end{aligned} \tag{11}$$

The optimization problem (11) is a non-differentiable convex quadratic programming (CQP) with NT linear equality constraints and $(4N + L)T$ linear inequality constraints. The number of variables are dependent on the numbers of charging vehicles. Centralized optimization algorithms may suffer from prohibitive issues such as communication, long computation time and privacy concerns, thus distributed methods are desirable to solve the problem.

3. Distributed charging control

In this section, based on the framework of ADMM [16], we propose a distributed charging control scheme for the SPCC model (11), in which each PEV user just implements a local computation by utilizing individual private information.

3.1. Problem reformulation based ADMM

The ADMM method has emerged as a powerful tool for large-scale structured optimization [16]. Notably, ADMM can decouple the spatially coupled constraints and decompose the original problem into many smaller sub-problems, in which each sub-problem is tackled easily.

Note that the first term in the objective of the model (11) couples all the variables $x_{n,t},\ n \in \mathcal{N}$. In order to decouple the term, we introduce an *auxiliary variable*,

$$\mathbf{x}_{N+1} = (x_{N+1,1}, \ldots, x_{N+1,T})^\top \in \mathbb{R}^T,$$

where $x_{N+1,t} = d_t + \sum_{n=1}^{N} x_{n,t}, \forall\ t \in \mathcal{T}$, thus, the problem (11) can be equivalently represented as

$$\min_{\mathbf{x} \in \mathcal{X}^{(1)}} \ G_\gamma(\mathbf{x}) \tag{12}$$

$$\text{s.t.} \ \sum_{n \in \Gamma_l} x_{n,t} \le c_{l,t},\ \ l \in \mathcal{L}, t \in \mathcal{T}, \tag{13}$$

$$d_t + \sum_{n=1}^{N} x_{n,t} = x_{N+1,t},\ \ \forall\ t \in \mathcal{T}. \tag{14}$$

To utilize the ADMM algorithm, we define

$$\mathbf{X} = (\mathbf{x}_1, \ldots, \mathbf{x}_N, \mathbf{x}_{N+1})^\top \in \mathbb{R}^{(N+1)\times T}. \tag{15}$$

We also write $\mathbf{X} = (\mathbf{x}_1, \ldots, \mathbf{x}_T) \in \mathbb{R}^{(N+1)\times T}$, where

$$\mathbf{x}_t = (x_{1,t}, \ldots, x_{N,t}, x_{N+1,t})^\top \in \mathbb{R}^{N+1},\ \ t \in \mathcal{T}.$$

Define

$$\mathcal{X}_t^{(2)} = \{\mathbf{x}_t \mid \mathbf{x}_t \text{ satisfies (13) and (14)}\},\ \ \forall t \in \mathcal{T}, \tag{16}$$

and

$$\mathcal{X}^{(2)} = \mathcal{X}_1^{(2)} \times \cdots \times \mathcal{X}_t^{(2)} \times \cdots \times \mathcal{X}_T^{(2)}, \tag{17}$$

where the constraint $\mathcal{X}^{(2)}$ is a global constraint, spatially coupling the charging schedules of all the PEVs. Note that $\mathcal{X}^{(1)} \cap \mathcal{X}^{(2)}$ is a compact, convex set. To make use of the ADMM method, we further introduce the indicator functions for the convex sets $\mathcal{X}^{(i)},\ i = 1, 2$, as follows,

$$\mathcal{I}_i(\mathbf{X}) = \begin{cases} 0, & \text{if } \ \mathbf{X} \in \mathcal{X}^{(i)}, \\ +\infty, & \text{otherwise.} \end{cases} \tag{18}$$

Clearly, $\mathcal{I}_i(\mathbf{X}), i = 1, 2$ are convex functions.

Now we are readily to write the problem described by (12)–(14) in a standard ADMM form as below

$$\begin{aligned} &\min_{\mathbf{X},\mathbf{Y}} \ G_\gamma(\mathbf{X}) + \mathcal{I}_1(\mathbf{X}) + \mathcal{I}_2(\mathbf{Y}) \\ &\text{s.t.} \ \ \mathbf{X} - \mathbf{Y} = 0. \end{aligned} \tag{19}$$

Applying the ADMM method to the problem (19) leads to

$$\mathbf{X}^{k+1} = \arg\min_{\mathbf{X}} \mathcal{L}_\rho\left(\mathbf{X}, \mathbf{Y}^k; \Lambda^k\right), \tag{20}$$

$$\mathbf{Y}^{k+1} = \arg\min_{\mathbf{Y}} \mathcal{L}_\rho\left(\mathbf{X}^{k+1}, \mathbf{Y}; \Lambda^k\right), \tag{21}$$

$$\Lambda^{k+1} = \Lambda^k + \rho\left(\mathbf{X}^{k+1} - \mathbf{Y}^{k+1}\right), \tag{22}$$

where

$$\mathcal{L}_\rho(\mathbf{X}, \mathbf{Y}; \Lambda) = G_\gamma(\mathbf{X}) + \mathcal{I}_1(\mathbf{X}) + \mathcal{I}_2(\mathbf{Y}) + \sum_{t \in \mathcal{T}} \Lambda_t^\top (\mathbf{X}_t - \mathbf{Y}_t) + \frac{\rho}{2} ||\mathbf{X} - \mathbf{Y}||_F^2 \tag{23}$$

is the augmented Lagrangian of the problem (19), $\Lambda \in \mathbb{R}^{(N+1)\times T}$ is the multiplier, $\rho > 0$ is a penalty parameter.

The convergence of ADMM iterations (20)–(22) is often characterized in terms of the residuals

$$r^{k+1} = ||\mathbf{X}^{k+1} - \mathbf{Y}^{k+1}||_F, \tag{24}$$

$$s^{k+1} = ||\rho\left(\mathbf{Y}^{k+1} - \mathbf{Y}^{k}\right)||_F, \tag{25}$$

named the primal and dual residuals at iteration $(k+1)$, respectively. The two residuals r^{k+1} and s^{k+1} converge to zero as ADMM proceeds [16]. This suggests a reasonable termination criterion that the primal and dual residuals must be small enough.

3.2. *X*-update by solving $(N+1)$ sub-problems

In this section we present a *distributed* implementation for the *X*-update in (20). From (20) and (23), we have

$$\begin{aligned}\mathbf{X}^{k+1} &= \arg\min_{\mathbf{X}\in\mathcal{X}^{(1)}} G_\gamma(\mathbf{X}) + \frac{\rho}{2}||\mathbf{X} - \mathbf{Y}^k + \mathbf{U}^k||_F^2 \\ &= \arg\min_{\mathbf{X}\in\mathcal{X}^{(1)}} \left\{ ||\mathbf{x}_{N+1}||_2^2 + \gamma\sum_{n=1}^{N}||\mathbf{x}_n||_1 + \frac{\rho}{2}\sum_{n=1}^{N+1}||\mathbf{x}_n - \mathbf{y}_n^k + \mathbf{U}_n^k||_2^2 \right\},\end{aligned} \tag{26}$$

where $\mathbf{U}_n^k = \Lambda_n^k/\rho$ is the scaled multiplier [16].

Interestingly, the optimization problem (26) can be further divided into $(N+1)$ sub-problems according to the definition of $\mathcal{X}^{(1)}$ in (8). More specifically, for $n = N+1$, the corresponding sub-problem has a closed-form solution, given by

$$\mathbf{x}_{N+1}^{k+1} = \frac{\rho}{\rho+2}\left(\mathbf{y}_{N+1}^k - \mathbf{U}_{N+1}^k\right), \tag{27}$$

and for $n = 1, \ldots, N$, the corresponding sub-problem is given by

$$\mathbf{x}_n^{k+1} = \text{argmin}_{\mathbf{x}_n\in\mathcal{X}_n^{(1)}}\left\{\gamma||\mathbf{x}_n||_1 + \frac{\rho}{2}||\mathbf{x}_n - \mathbf{y}_n^k + \mathbf{U}_n^k||_2^2\right\}. \tag{28}$$

Remark 1. (1) The optimization sub-problem (28) is a small-scale CQP problem (T dimension) subject to the local linear constraints (3)–(6), which is easily solved by convex optimization methods or solvers. (2) The corresponding sub-problem (28) is solved by each user in a parallel manner, only requiring the private information of individual PEV user accessible, thus, PEV user's privacy can be protected. (3) The term in (28) involving ℓ_1-minimization can improve the customers' satisfaction by characterizing the sparsity of charging schedules [38].

3.3. Accelerated *Y*-update by solving T sub-problems

Now we consider a *distributed* implementation for the **Y**-update in (21). From (21) and (23), we obtain

$$\begin{aligned}\mathbf{Y}^{k+1} &= \arg\min_{\mathbf{Y}} \mathcal{I}_2(\mathbf{Y}) + \frac{\rho}{2}||\mathbf{X}^{k+1} - \mathbf{Y} + \mathbf{U}^k||_F^2 \\ &= \arg\min_{\mathbf{Y}\in\mathcal{X}^{(2)}} \frac{\rho}{2}||\mathbf{Y} - \left(\mathbf{X}^{k+1} + \mathbf{U}^k\right)||_F^2.\end{aligned} \tag{29}$$

According to the definition of $\mathcal{X}^{(2)}$ in (17), the problem (29) can be further divided into the following T sub-problems separately, that is, for $t = 1, \ldots, T$

$$\min_{\mathbf{y}_t\in\mathcal{X}_t^{(2)}}\left\{\mathbf{y}_t^\top\mathbf{y}_t - 2\left(\mathbf{x}_t^{k+1} + \mathbf{U}_t^k\right)^\top\mathbf{y}_t\right\}. \tag{30}$$

The sub-problem (30) is a CQP problem, which can be solved by traditional optimization techniques, e.g., interior point method. However, when the number of PEVs plugged in the network becomes larger, the centralized control is infeasible to gather all the information of PEVs. Moreover, most of PEV consumers may be unlike to reveal the privacy to the others. Therefore, it is necessary to develop a distributed algorithm for solving the sub-problem (30).

For notational simplicity, we introduce a $(L\times N)$-matrix $\mathbf{A}^t$ to represent the feeder-user incidence matrix at time t with its component $a_{l,n}^t$, defined by

$$a_{l,n}^t = \begin{cases} 1, & \text{if PEV } n \text{ uses feeder } l \text{ at time } t, \\ 0, & \text{otherwise.}\end{cases}$$

Let $\mathbf{A}^t = (\mathbf{a}_1^t, \ldots, \mathbf{a}_N^t)$ ($\mathbf{a}_n^t$ is the nth column vector of $\mathbf{A}^t$, representing the corresponding feeders that PEV n uses), $\mathbf{a}_{N+1}^t = \mathbf{0} \in \mathbb{R}^L$, $\mathbf{c}^t = (c_{1,t}, \ldots, c_{L,t})^\top$, $b_n = -1, n \in \mathcal{N}, b_{N+1} = 1$. Then, we rewrite the sub-problem (30) as follows,

$$\begin{aligned}&\min \sum_{n=1}^{N+1} y_{n,t}^2 - 2\left(x_{n,t}^{k+1} + U_{n,t}^k\right)y_{n,t} \\ &\text{s.t.} \sum_{n=1}^{N+1}\mathbf{a}_n^t y_{n,t} \le \mathbf{c}^t,\end{aligned}$$

$$\sum_{n=1}^{N+1} b_n y_{n,t} = d_t. \tag{31}$$

For each fixed $t \in \mathcal{T}$, we now focus on solving the sub-problem (31). In order to decouple the coupled constraints in the sub-problem (31), we introduce the Lagrangian of (31)

$$\begin{aligned}\mathcal{L}^t(\mathbf{y}_t; \lambda_t, \mu_t) &= \sum_{n=1}^{N+1} \left[y_{n,t}^2 - 2\left(x_{n,t}^{k+1} + U_{n,t}^k\right) y_{n,t}\right] + \lambda_t^\top \left[\mathbf{a}_n^t y_{n,t} - \mathbf{c}^t/(N+1)\right] + \mu_t [b_n y_{n,t} - d_t/(N+1)] \\ &:= \sum_{n=1}^{N+1} \mathcal{L}_n^t(\mathbf{y}_t; \lambda_t, \mu_t),\end{aligned} \tag{32}$$

where $\lambda_t = (\lambda_{1,t}, \ldots, \lambda_{L,t})^\top \in \mathbb{R}_+^L$ and $\mu_t \in \mathbb{R}$ are dual (price) variables. Further, we refer to $\lambda_{l\ t}$ as the *feeder-price* when the PEV uses the feeder l at time t, and μ_t as the virtual supply-demand *balance-price*. Note that the Lagrangian $\mathcal{L}^t(\mathbf{y}_t; \lambda_t, \mu_t)$ defined in (32) is separable with respect to $y_{1,t}, \ldots, y_{N+1,t}$.

The dual problem of (31) is

$$\max_{\lambda_t \geq \mathbf{0}, \mu_t} \left\{\mathcal{D}^t(\lambda_t, \mu_t) := \min_{\mathbf{y}_t} \mathcal{L}^t(\mathbf{y}_t; \lambda_t, \mu_t)\right\}. \tag{33}$$

According to (32), the dual objective can be written as the following separable form

$$\mathcal{D}^t(\lambda_t, \mu_t) = \sum_{n=1}^{N+1} \min_{y_{n,t}} \mathcal{L}_n^t(\mathbf{y}_t; \lambda_t, \mu_t).$$

The *separability* of $\mathcal{D}^t$ gives rise to an optimized scheme that all the PEV users can simply self-optimized in a parallel manner. Furthermore, since the objective function for the problem (31) is strongly convex, we have provable properties [42]: (i) $\mathcal{D}^t$ is concave, (ii) $\mathcal{D}^t$ is differentiable, and (iii) the gradient

$$\nabla \mathcal{D}^t = \left(\nabla_{\lambda_t} \mathcal{D}^t, \nabla_{\mu_t} \mathcal{D}^t\right)^\top$$

is L_t-Lipschitz continuous, where

$$\nabla_{\lambda_t} \mathcal{D}^t = \sum_{n=1}^{N+1} \mathbf{a}_n^t y_{n,t}(\lambda_t, \mu_t) - \mathbf{c}^t, \quad \nabla_{\mu_t} \mathcal{D}^t = \sum_{n=1}^{N+1} b_n y_{n,t}(\lambda_t, \mu_t) - d_t,$$

and

$$y_{n,t}(\lambda_t, \mu_t) = \arg\min_{y_{n,t}} \mathcal{L}_n^t(\mathbf{y}_t; \lambda_t, \mu_t), n = 1, \ldots, N+1. \tag{34}$$

Based on these properties and our previous work [42], an accelerated gradient method is proposed to solve the dual problem (33) presented in Algorithm 1, in which the solutions of the primal problem (31) can be obtained simultaneously.

Remark 2. In Algorithm 1, the system-prices compose of the feeder-price and the balance-price. In Step 7, each PEV user $n \in \mathcal{N}$ updates its schedule only by the aggregated feeder-price $(\xi_l^\tau)_{l \in \Pi_n}$ for the feeders that service this PEV user. In Step 11, each feeder $l \in \mathcal{L}$ updates its price only by the aggregated loads $(y_{n,t}^\tau)_{n \in \Gamma_l}$ for the users that utilize this feeder. Thus, all the updates are run in a completely distributed manner by using local information accessible to each user or feeder.

3.4. Distributed charging control algorithm

For clarity, we summarize the above procedures in Algorithm 2 for solving the SPCC model (11) in a distributed way based on the framework of ADMM. Note that the Λ-update in (22) can be computed locally by Step 8 of Algorithm 2.

Remark 3. The distributed charging control algorithm presented in Algorithm 2 is scalable. Once the problem formulations satisfying that the objective is convex subject to both globally and locally linear constraints, our proposed algorithm can be suitable to solve them. Several formulations of PEV charging control problems, for examples, the valley-fill charging model described in [11] and the cost-minimal charging model incorporating battery degradation cost proposed in [35], can be solved by applying our Algorithm 2.

Now we provide the convergence analysis of the proposed algorithms. We first obtain the following Proposition 1 to show the convergence characteristics for Algorithm 2. The proof of Proposition 1 is given in Appendix A.1.

Proposition 1. *Let the sequence* $\{(\mathbf{X}^k, \mathbf{Y}^k; \Lambda^k)\}$ *be generated by Algorithm 2, then, for the problem (19) in a ADMM form (equivalent to the SPCC model (11)), we have*

(1) *residual convergence:* $\max(r^{k+1}, s^{k+1}) \to 0$ *as* $k \to \infty$,
(2) *objective convergence: the objective function of the iterates converges to the optimal value.*

Algorithm 1 **Y**-Update by Accelerated Dual Gradient Algorithm.

procedure $\mathbf{y}_t^{k+1} :=$ ACCELERATED-$\mathbf{Y}(\mathbf{X}^{k+1}, \Lambda^k)$

Initialization: for each fixed $t \in \mathcal{T}$, given parameters $\theta^0 = \theta^{-1} = 1$ and $0 < \alpha_t \le 1/L_t$; set feeder-price $\lambda_{l,t}^0 = \lambda_{l,t}^{-1} \ge 0, l \in \mathcal{L}$ and balance-price $\mu_t^0 = \mu_t^{-1}$; set $\tau := 0$;

repeat

Accelerate system-prices: for all $l \in \mathcal{L}$

$$\xi_{l,t}^{\tau} := \lambda_{l,t}^{\tau} + \theta^{\tau}(1/\theta^{\tau-1} - 1)(\lambda_{l,t}^{\tau} - \lambda_{l,t}^{\tau-1});$$

$$\zeta_t^{\tau} := \mu_t^{\tau} + \theta^{\tau}(1/\theta^{\tau-1} - 1)(\mu_t^{\tau} - \mu_t^{\tau-1});$$

for each PEV $n = 1, \ldots, N+1$ **do**

Receive aggregated prices $(\xi_l^{\tau})_{l \in \Pi_n}$ and ζ_t^{τ};

Update *individual charging schedule*

$$y_{n,t}^{\tau} := \arg\min_{y_{n,t}} \mathcal{L}_n^t(y_{n,t}; (\xi_l^{\tau})_{l \in \Pi_n}, \zeta_t^{\tau});$$

end for

for each feeder $l = 1, \ldots, L$ **do**

Receive aggregated schedules $(y_{n,t}^{\tau})_{n \in \Gamma_l}$;

Update *system-prices*: for all $l \in \mathcal{L}$

$$\lambda_{l,t}^{\tau+1} := \left[\xi_{l,t}^{\tau} + \alpha_t \nabla_{\lambda_{l,t}} \mathcal{D}^t((y_{n,t}^{\tau})_{n \in \Gamma_l})\right]_+;$$

$$\mu_t^{\tau+1} := \zeta_t^{\tau} + \alpha_t \nabla_{\mu_t} \mathcal{D}^t((y_{n,t}^{\tau})_{n \in \Gamma_l});$$

end for

Update $\theta^{\tau+1} := [\sqrt{(\theta^{\tau})^4 + 4(\theta^{\tau})^2} - (\theta^{\tau})^2]/2$;

Set $\tau := \tau + 1$;

until a preset stopping criterion is met

return $\mathbf{y}_t^{k+1} := \mathbf{y}_t^{\tau}$.

end procedure

Algorithm 2 Distributed Charging Control Algorithm for SPCC Model (11).

procedure $\mathbf{X}^{k+1}$:=D-CHARGING$(\mathbf{Y}^0, \Lambda^0)$

Initialization: set accuracy $\epsilon > 0$, penalty parameter $\rho > 0$; initial values $\mathbf{Y}^0, \Lambda^0 \in \mathbb{R}^{(N+1)\times T}$; set $k := 0$;

repeat

X-*update:*

for $n = 1, \ldots, N$, update $\mathbf{x}_n^{k+1}$ by solving (28), and

for $n = N+1$, update $\mathbf{x}_{N+1}^{k+1}$ by (27);

Y-*update:* for $t = 1, \ldots, T$, update

$$\mathbf{y}_t^{k+1} := \text{ACCELERATED-}\mathbf{Y}(\mathbf{X}^{k+1}, \Lambda^k) \text{ by } \textbf{Algorithm 1};$$

Λ-*update:* for $n = 1, \ldots, N+1,\ t = 1, \ldots, T$,

$$\Lambda_{n,t}^{k+1} := \Lambda_{n,t}^{k} + \rho(x_{n,t}^{k+1} - y_{n,t}^{k+1}) \text{ by (22)};$$

Set $k := k + 1$;

until $\max(r^{k+1}, s^{k+1}) \le \epsilon$;

return $\mathbf{X}^{k+1}$.

end procedure

Next we show the convergence properties for Algorithm 1, presented in Proposition 2. The proof of Proposition 2 is given in Appendix A.2.

Proposition 2. *For each fixed $t \in \mathcal{T}$, let (λ_t^*, μ_t^*) and $\mathbf{y}_t^*$ be the dual and primal solutions of the sub-problem (31). Let $\{(\lambda_t^{\tau}, \mu_t^{\tau})\}$ and $\{\mathbf{y}_t^{\tau}\}$ be the sequences generated by Algorithm 1. Then, for all $\tau \ge 0$, we have*

(1) $\mathcal{D}^t(\lambda_t^*, \mu_t^*) - \mathcal{D}^t(\lambda_t^{\tau+1}, \mu_t^{\tau+1}) \le C/(\tau+2)^2$,
(2) $||\mathbf{y}_t^{\tau+1} - \mathbf{y}_t^*||_2 \le \sqrt{C}/(\tau+2)$,

where $C = 2L_t||(\lambda_t^0, \mu_t^0) - (\lambda_t^*, \mu_t^*)||_2^2$ is a constant.

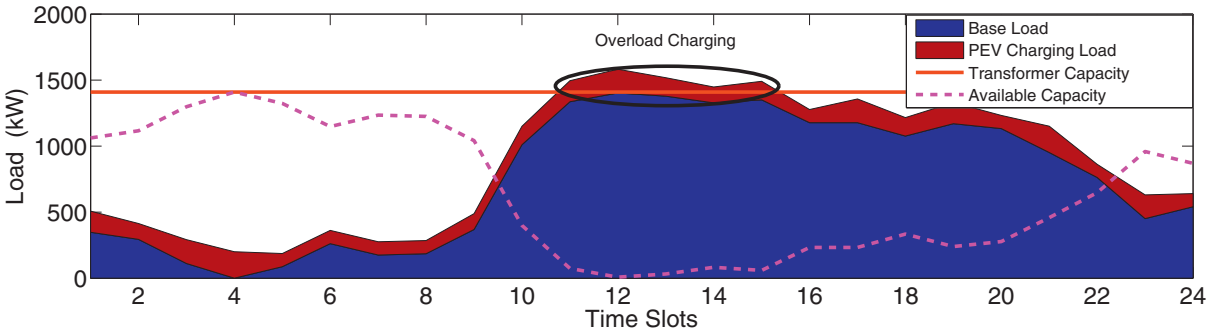

Fig. 2. SPCC coordination without overload control: the base load plus the charging requirement of PEVs over 24 hourly time slots at node 671.

The result (1) of Proposition 2 indicates that the sequence of dual objectives generated by Algorithm 1 can converge to the dual optimal value within the rate of convergence $\mathcal{O}(1/\tau^2)$, in which the convergence rate is proved to be optimal, and faster than dual subgradient-based methods [42]. In addition, we prove a new convergence result (2) of Proposition 2, which indicates that the sequence of primal solutions can converge to the primal solution with a rate $\mathcal{O}(1/\tau)$.

4. Numerical experiments

In this section we report and illustrate some experimental results on the performances of the proposed algorithms as well as making comparisons with existing algorithms.

4.1. Overload control of feeders

In the simulation, the tree structured distribution network with IEEE Bus 13 [43] is used, also see Fig. 1. As usual, the time slots from 10:00 to 20:00 are assumed to be peak hours and the electric bill is b=0.80$/kWh. The time intervals from 0:00 to 8:00 and from 22:00 to 24:00 are off peak hours with b=0.60$/kWh. The remaining time slots are shoulder hours with b=0.70$/kWh. The data of hourly load demand with a typical day in summer is adapted from [44].

We set the capacity of each feeder l as $C_l = \eta R_l D^{\max}$, where $D^{\max}$ is the maximum generation capacity of the distribution network, R_l is the *spot load ratio* for the feeder l (base load on feeder l as a fraction of total base load in network) derived from [44], η is the safety factor. We calculate the base load of the feeder l by $D_{l,t} = R_l d_t$. Thus, for each feeder, the maximum excess power that can be used for charging PEVs is

$$c_{l,t} = C_l - D_{l,t} = R_l(\eta D^{\max} - d_t).$$

It follows from the above equation that the excess power of each feeder that can be used for charging PEVs is time-varying. We let $G_0 = \sum_{t\in\mathcal{T}}(d_t + \sum_{n\in\mathcal{N}} \mathbf{x}_{n,t})^2$ to represent the variance of the total load, corresponding to G_γ defined in (11) with $\gamma = 0$.

4.1.1. Overload control on a feeder

In this experiment, we assume that there are 30 PEVs with homogeneous charging constraints connected to a typical node 671 (load bus or transformer) of IEEE Bus 13 network. We set $\eta = 1.2$ and $D^{\max} = 5$ MW. The capacity of the transformer 671 is 1410 kW. The charging demand for each PEV is set as 50 kWh. The maximum charging rate for each PEV is set as 8 kW. The initialized charging requirement for each PEV is randomly generated. For simplicity, we consider the case without the sparsity by setting $\gamma = 0$.

We now use the SPCC model (11) to coordinate the PEV charging by utilizing the proposed algorithms in this paper. In the following, we investigate two cases.

(1) No overload control on the feeders: we investigate the SPCC model (11) without the feeder constraints (9). As shown in Fig. 2, the magenta dash line is the maximal capacity available at the node 671 that supports the PEV charging. The blue and the brown areas are the base load and the charging requirement load over 24 time slots, respectively. From 10:00 to 21:00, there are peak-hours. It can be observed from this figure that the summation of the base load and the aggregated charging strategy exceeds the transformer capacity from 11:00 to 15:00. In this case, the node 671 has appeared overloads due to the lack of overload control on feeders, which possibly poses security issue to the distribution network. In addition, the variance of the total load G_0 is 14.735 MW^2.

(2) Overload control on the feeders: we investigate the SPCC model (11) subjected to the feeder constraints (9). The results of shifting load are displayed in Fig. 3 in the same feasible zone, where the charging schedules always stay below the maximal capacity of the transformer. This implies that the proposed overload control strategy can ensure the operational security of distribution feeders and transformers. Under this case, the variance of the total load G_0 is 14.740 MW^2. Clearly, the variance with feeder overload control does not obviously increase when compared with the variance without feeder overload control.

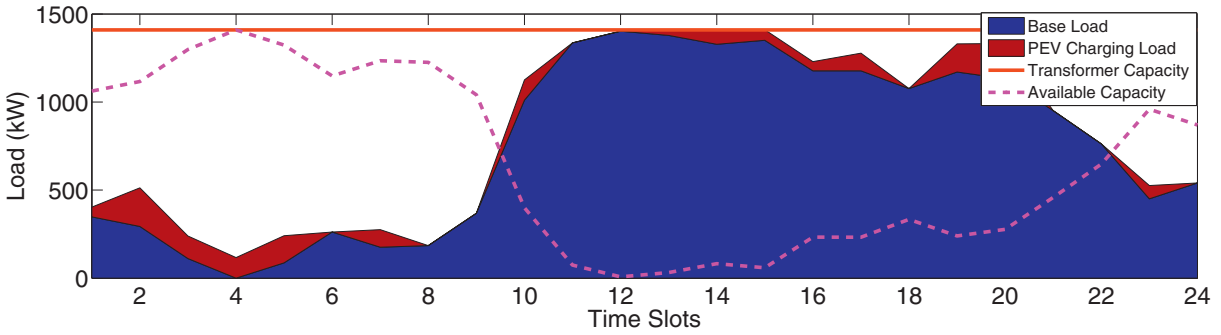

Fig. 3. SPCC coordination with overload control: the base load plus the charging requirement of PEVs with overload control over 24 hourly time slots at node 671.

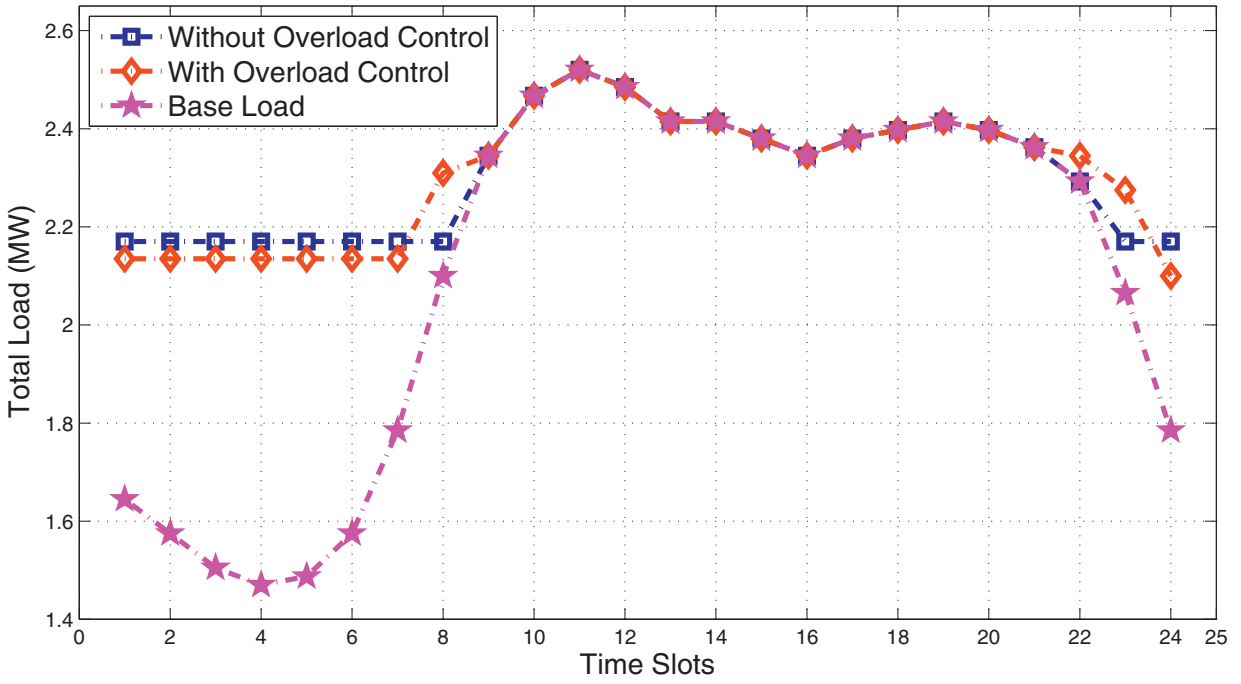

Fig. 4. SPCC coordination: total load without overload control, total load with overload control, and the base load.

4.1.2. Overload control on all feeders

In this section we consider a more complex and larger case, in which each leaf node of the network IEEE Bus 13 is attached to different categories of PEVs with 200 PEVs. We consider that each leaf node supports 100 home chargers and 100 office chargers. We assume that all the home chargers charge 12 kWh of energy with maximum power rate of 1.96 kW, only allowed to be charged between 6 pm and 7 am, and the office chargers charge 13 kWh of energy with the maximum power rate of 7.2 kW, only allowed to be charged from 8 am and 5 pm [33]. In this case, let the feeder safety parameter $\eta = 2.0$. The initialized load profiles of all PEVs are generated randomly. To monitor the feeder overload in the network, we introduce the normalized maximum overload of the feeders, calculated by, for each $t \in \mathcal{T}$

$$\text{Normalized Maximum Overload} := \max_{l \in \mathcal{L}} \frac{\sum_{n \in \Gamma_l} x_{n,t} - c_{l,t}}{c_{l,t}}.$$

In the following, we use the proposed Algorithm 2 to solve the SPCC model (11). Under the SPCC coordination, we still consider two scenarios: without feeder overload control and with feeder overload control.

Figs. 4 and 5 display the total load and normalized maximum overload, respectively. By Fig. 4, it can be seen that the variances of the total load with feeder overload control are quite close to those with no overload control. In addition, the results of Fig. 4 demonstrate that the valley of the load curve can be effectively filled up by the proposed algorithms in both cases.

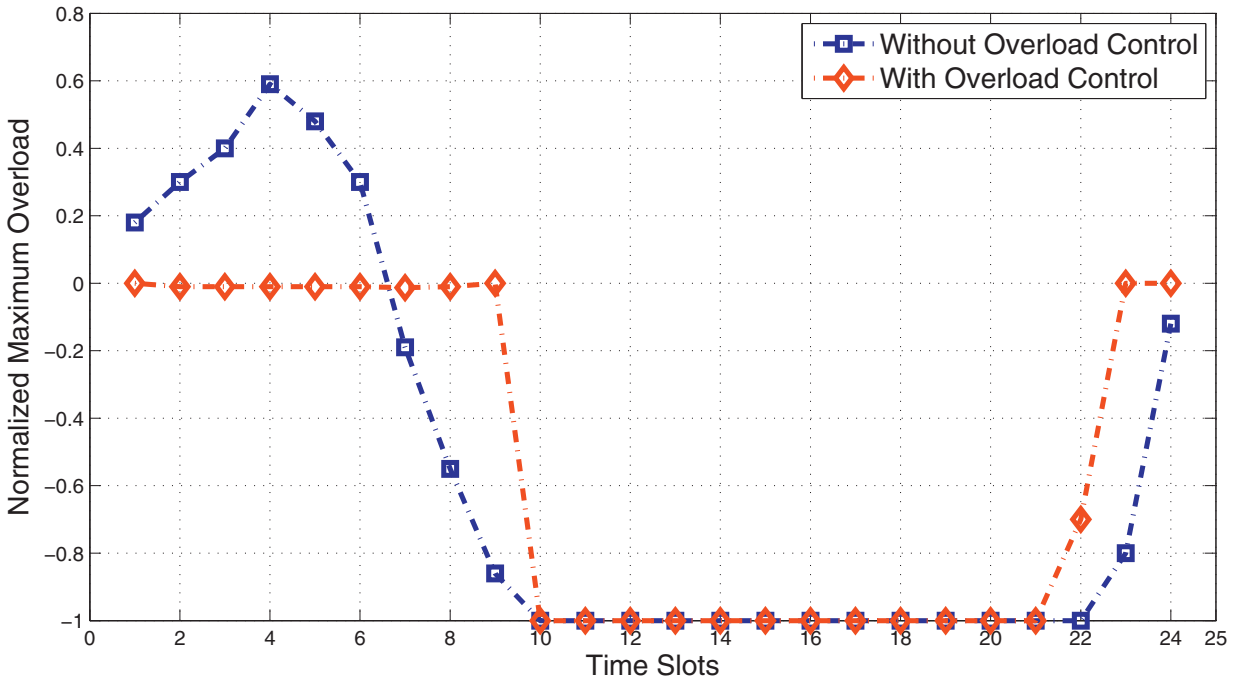

Fig. 5. SPCC coordination: normalized maximum overload without feeder overload control and normalized maximum overload with feeder overload control.

By Fig. 5, it can be observed that the normalized overload always stays below zero or very close to it at all time slots with feeder overload control. But the solution of no overload control does apparently overload one or more of the feeders over some time slots. By the simulation experiments, it can concluded that the SPCC coordination is effective to avoid overloading of feeders. Moreover, the proposed Algorithm 2 is efficient for the two cases. As seen from Fig. 5, the feeder overload occurs when the total load is low while taking no account of the feeder limits. This would be explained that each PEV consumer tries to minimize the charging cost, and the user possibly spread the charging schedule over the minimum total load time periods.

4.2. Sparsity pattern of customers' satisfaction

In this section, we evaluate the performance of the proposed approach by exploiting the sparsity pattern to improve customers' satisfaction. As explained in Section 2, the fewer charging time slots, the greater customers' satisfaction. Hence, if the solution of the SPCC model (11) is sparse enough, the proposed distributed charging control strategy will satisfy all customers in the sense of comfort and minimal variance.

Consider, for example, there are 10 PEVs connecting to the node 671. To reveal the sparsity pattern more precisely, we use 30 min as a time slot, i.e., 48 time slots per day. For simplicity, we assume that the safety factor η is appropriately large and the feeder constraints (9) are automatically satisfied. In order to assess the sparse charging control strategy in this case, we define the following sparsity level (SL) ,

$$\mathrm{SL} := \frac{\sum_{n=1}^{N} ||\mathbf{h}_n||_0 - \sum_{n=1}^{N} ||\mathbf{x}_n^*||_0}{\sum_{n=1}^{N} ||\mathbf{h}_n||_0} \times 100\%,$$

where $\mathbf{x}_n^*$ represents the sparse charging schedules of PEV n obtained by solving the model (11) using Algorithm 2, and $\mathbf{h}_n$ presents the feasible time slots for PEV n.

As shown in Fig. 6, each blue triangle represents that the PEV is being charged in this time slot. By applying sparse charging control, only 174 time slots are used to minimize the objective function $G_\gamma(\mathbf{x})$ defined in (11) by letting $\gamma = 0.10$, whereas 268 time slots are occupied by satisfying the feasible constraints. Thus, the sparsity level is 35.07%. Clearly, all the PEVs will experience fewer charging slots, which means that each PEV user will be less disrupted via the sparsity pattern control. Note that the value G_γ is 13.11 MW^2 with $\gamma = 0.10$, while the total load variance G_0 is 12.52 MW^2 if there was no sparsity strategy applied. Although the amount G_γ under the sparsity pattern brings a 0.59 MW^2 extra cost for all PEV customers, the sparsity pattern for the proposed method can reduce the numbers of charging slots and bring more customers' satisfaction.

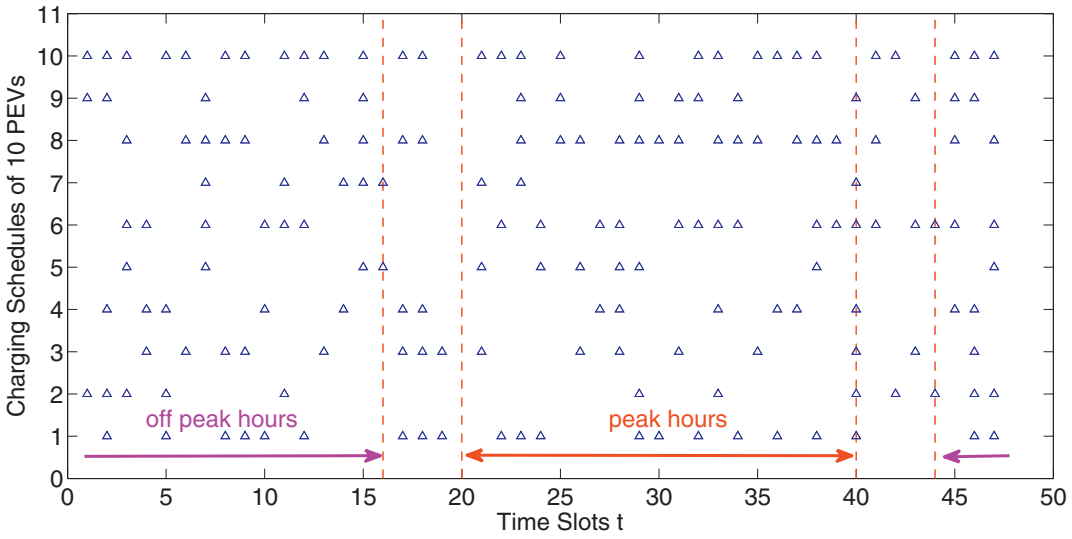

Fig. 6. Sparsity pattern of 10 PEVs with respect to distributed charging control strategy.

Table 2
The sparsity level with different γ.

γ	0.01	0.05	0.10	0.50	1.00
SL(%)	22.74	30.78	35.07	36.91	38.02

Table 3
The results with different numbers of PEVs.

	N	50	100	200	400	800
CPU	Algorithm PDSG	4.30	6.70	21.30	50.50	89.20
	Algorithm 2	3.10	4.80	7.90	15.70	27.30
G_γ	Algorithm PDSG	19.91	32.43	58.45	88.05	130.11
	Algorithm 2	19.91	32.30	57.85	87.79	129.75

Table 2 shows the results of the sparsity level with different values of the weighing parameter γ. It can be observed that the sparsity level gradually increases as the parameter γ becomes big. This shows that the value of weighing parameter γ has a potential influence on the sparsity of the charging schedules.

4.3. Convergence performance of proposed algorithms

In the section, we make some performance comparisons between the proposed algorithms and several existing algorithms [11,32]. More specifically, we compare the performance between Algorithm 2 and the primal-dual subgradient (PDSG) algorithm proposed in [32], Algorithm 1 and the standard gradient-based dual ascend (GDA) algorithm proposed in [11], respectively.

4.3.1. Comparisons between Algorithms 2 and PDSG

Now we investigate the case, where different numbers of PEVs are attached to the leaf node 671 for charging in the distribution network. For simplicity, we assume that the leaf node 671 only supports office chargers. We let the office chargers charge 13 kWh of energy with the maximum power rate of 7.2 kW. The periods of time for charging office changers are set from 8 am and 5 pm. We set $\gamma = 0.10$ and $\eta = 1.5$. In order to compare, we set the accuracy $\epsilon = 0.10$ or the allowed maximum iterations $k_{\max} = 5e4$ as the stopping criterion for two algorithms.

Table 3 illustrates the numerical results between Algorithm 2 and PDSG in terms of the computational time (CPU) in second and the values of objective function G_γ defined in (11). The results in Table 3 show that two algorithms take more computational time as the numbers of PEV users N increase. By comparison, Algorithm 2 are much faster than Algorithm PDSG in all cases. In terms of the values of objective function, both algorithms almost achieve the same results, but the values of Algorithm 2 obtained are slightly smaller than those of Algorithm PDSG obtained in most cases.

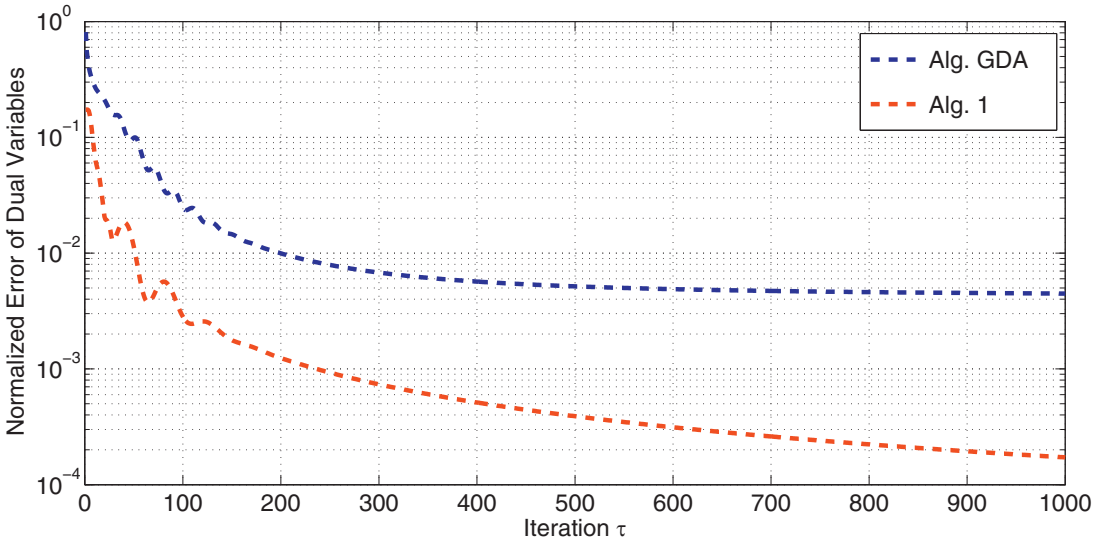

Fig. 7. Comparison of the convergence performance for Algorithm 1 and GDA.

4.3.2. Comparisons between Algorithms 1 and GDA

In the section, the performance of Algorithm 1 for solving the sub-problem (31) is investigated. In order to compare, we denote the normalized error of dual variables, given by

$$\text{Normalized Error} := \frac{\|(\lambda_t^\tau, \mu_t^\tau) - (\lambda_t^*, \mu_t^*)\|_2}{\|(\lambda_t^*, \mu_t^*)\|_2},$$

where the (λ_t^*, μ_t^*) is the dual optimal solution of the problem (31). The same data settings in the Section 4.1 are adapted, with $N = 30$, $\gamma = 0.10$ and $t = 10$. We compare the normalized error of dual variables between the proposed Algorithm 1 and Algorithm GDA, shown in Fig. 7. After 300 iterations, the computational accuracy of Algorithm 1 is better than that of Algorithm GDA. It can be seen from Fig. 7 that Algorithm 1 can indeed arrive at a desirable accuracy 0.001 within 300 iterations while Algorithm GDA in [11] only converges at an accuracy 0.005 more than 700 iterations.

5. Conclusion

In this paper, we proposed a sparsity-promoting control model for coordinately charging PEVs subject to feeder overload constraints over a distribution network. The main contribution was to introduce a sparsity-promoting charging pattern to control PEV charging. The advantage of this method is that it can reduce the numbers of charging time slots significantly through sparsity optimization. In simulations, the occupied charging time slots for 10 PEVs was reduced from 268 to 174 by using our sparsity-promoting pattern. Thus, the consumer satisfaction for PEV owners can be improved significantly [38].

This paper models the charging rate of the PEVs as a continuous variable, future work will look at a discrete formulation by modeling the charging rate of the PEVs as a binary variable. Bi-objective model is also worth to investigate in future since our model is relied on the wight in the objective function.

A.1. Proof of Proposition 1

Proof. With a similar argument from Section 3.2.1 in [16], we will verify that both primal residual r^k and dual residual s^k converge to zero as $k \to \infty$. Then, we will obtain the objective convergence, i.e., the objective p^k converges to the optimal value p^* of the problem (19) as $k \to \infty$, where $p^k = G_\gamma(\mathbf{X}^k) + \mathcal{I}_1(\mathbf{X}^k) + \mathcal{I}_2(\mathbf{Y}^k)$.

Let $\mathcal{L}_0(\mathbf{X}, \mathbf{Y}; \Lambda)$ be the Lagrangian of the problem (19) defined in (23) with $\rho = 0$. Let $(\mathbf{X}^*, \mathbf{Y}^*; \Lambda^*)$ be a saddle point for $\mathcal{L}_0$. We introduce the following Lyapunov function for Algorithm 2:

$$V^k = (1/\rho)||\Lambda^k - \Lambda^*||_F^2 + \rho||\mathbf{Y}^k - \mathbf{Y}^*||_F^2. \tag{35}$$

From (A.1) in [16], we have the inequality below:

$$\rho\left(||\mathbf{X}^{k+1} - \mathbf{Y}^{k+1}||_F^2 + ||\mathbf{Y}^{k+1} - \mathbf{Y}^k||_F^2\right) \le V^k - V^{k+1}, \tag{36}$$

which shows that V^k decreases in each iteration by an amount that depends on the norm of primal residual and the change in $\mathbf{Y}$ over one iteration. Note that both Λ^k and $\mathbf{Y}^k$ are bounded due to the fact that $V^k \le V^0$ and the update (22). Thus,

iterating the inequality (36) leads to

$$\rho \sum_{k=0}^{\infty} \left(||\mathbf{X}^{k+1} - \mathbf{Y}^{k+1}||_F^2 + ||\mathbf{Y}^{k+1} - \mathbf{Y}^{k}||_F^2 \right) \leq V^0, \tag{37}$$

which implies that $r^{k+1} \to 0$ and $s^{k+1} \to 0$ as $k \to \infty$. Therefore, the result (1) of the proposition is obtained.

Since $(\mathbf{X}^*, \mathbf{Y}^*; \Lambda^*)$ is a saddle point for $\mathcal{L}_0$, we have

$$\mathcal{L}_0(\mathbf{X}^*, \mathbf{Y}^*; \Lambda^*) \leq \mathcal{L}_0\left(\mathbf{X}^{k+1}, \mathbf{Y}^{k+1}; \Lambda^*\right). \tag{38}$$

Using $\mathbf{X}^* - \mathbf{Y}^* = 0$, it follows that $\mathcal{L}_0(\mathbf{X}^*, \mathbf{Y}^*; \Lambda^*) = p^*$. Together with the definition of p^k, the inequality (38) gives rise to

$$p^* - p^{k+1} \leq \sum_{t \in \mathcal{T}} \Lambda_t^{*\top} \left(\mathbf{X}_t^{k+1} - \mathbf{Y}_t^{k+1} \right) \leq r^{k+1} ||\Lambda^*||_F. \tag{39}$$

The righthand side in (39) goes to zero as $k \to \infty$, since r^{k+1} goes to zero. Following (A.2) in [16], we get the following inequality:

$$\begin{aligned} p^{k+1} - p^* &\leq -\sum_{t \in \mathcal{T}} \left(\Lambda_t^{k+1} \right)^\top \left(\mathbf{X}_t^{k+1} - \mathbf{Y}_t^{k+1} \right) - \rho \sum_{t \in \mathcal{T}} \left(\mathbf{Y}_t^{k+1} - \mathbf{Y}_t^{k} \right)^\top \left[\left(\mathbf{Y}_t^{k+1} - \mathbf{Y}_t^{*} \right) - \left(\mathbf{X}_t^{k+1} - \mathbf{Y}_t^{k+1} \right) \right] \\ &\leq r^{k+1} ||\Lambda^{k+1}||_F + s^{k+1} \left(||\mathbf{Y}^{k+1} - \mathbf{Y}^*||_F + r^{k+1} \right). \end{aligned} \tag{40}$$

The righthand side in (40) goes to zero as $k \to \infty$, because both Λ^k and $\mathbf{Y}^k$ are bounded, and $\max(r^{k+1}, s^{k+1}) \to 0$. Thus, we obtain $\lim_{k \to \infty} p^{k+1} = p^*$, which proves the objective convergence. □

A.2. Proof of Proposition 2

Proof. For notational simplicity, we let $f(\mathbf{y}_t) = \sum_{n=1}^{N+1} [y_{n,t}^2 - 2(x_{n,t}^{k+1} + U_{n,t}^k) y_{n,t}]$, $\mathbf{g}(\mathbf{y}_t) = \sum_{n=1}^{N+1} \mathbf{a}_n^t y_{n,t} - \mathbf{c}^t$ and $h(\mathbf{y}_t) = \sum_{n=1}^{N+1} b_n y_{n,t} - d_t$. For each fixed time slot $t \in \mathcal{T}$, let the sequence $\{\lambda_t^\tau, \mu_t^\tau, y_t^\tau, \theta^\tau\}_{\tau \geq 0}$ be generated by Algorithm 1.

We first prove the result (1) of the proposition.

Since the objective function $f(\mathbf{y}_t)$ is strongly convex over $\mathcal{X}_t$, the dual function $\mathcal{D}^t(\lambda_t, \mu_t)$ defined in (33) is concave and differentiable, and the gradient $\nabla \mathcal{D}^t(\lambda_t, \mu_t)$ is L_t-Lipschitz continuous. Following a similar argument with Lemma 2 in [42], we have, for any $\tau \geq 0$ and $(\lambda_t, \mu_t) \in \mathbb{R}_+^L \times \mathbb{R}$,

$$\begin{aligned} &\frac{\mathcal{D}^t(\lambda_t, \mu_t) - \mathcal{D}^t\left(\lambda_t^{\tau+1}, \mu_t^{\tau+1}\right)}{(\theta^\tau)^2} + \frac{L_t}{2} \|(\lambda_t, \mu_t) - \left(v_t^{\tau+1}, \omega_t^{\tau+1}\right)\|^2 + \frac{\triangle_{\mathcal{D}^t}\left(\lambda_t, \mu_t; \xi_t^\tau, \zeta_t^\tau\right)}{\theta^\tau} \\ \leq\ &\frac{1 - \theta^\tau}{(\theta^\tau)^2} \left(\mathcal{D}^t(\lambda_t, \mu_t) - \mathcal{D}^t(\lambda_t^\tau, \mu_t^\tau) \right) + \frac{L_t}{2} \|(\lambda_t, \mu_t) - (v_t^\tau, \omega_t^\tau)\|^2, \end{aligned} \tag{41}$$

where

$$\triangle_{\mathcal{D}^t}(\lambda_t, \mu_t; \xi_t^\tau, \zeta_t^\tau) = \mathcal{D}^t(\xi_t^\tau, \zeta_t^\tau) + \nabla \mathcal{D}^t(\xi_t^\tau, \zeta_t^\tau)^\top [(\lambda_t, \mu_t) - (\xi_t^\tau, \zeta_t^\tau)] - \mathcal{D}^t(\lambda_t, \mu_t)$$

and

$$\begin{aligned} (v_t^\tau, \omega_t^\tau) &= \left(\lambda_t^{\tau-1}, \mu_t^{\tau-1}\right) + \frac{1}{\theta^{\tau-1}} \left[(\lambda_t^\tau, \mu_t^\tau) - \left(\lambda_t^{\tau-1}, \mu_t^{\tau-1}\right) \right] \\ &= (\lambda_t^\tau, \mu_t^\tau) + \frac{1}{\theta^\tau} [(\xi_t^\tau, \zeta_t^\tau) - (\lambda_t^\tau, \mu_t^\tau)]. \end{aligned}$$

Note that $(v_t^0, \omega_t^0) = (\lambda_t^0, \mu_t^0)$ due to $(\lambda_t^0, \mu_t^0) = (\lambda_t^{-1}, \mu_t^{-1})$ from Step 2 of Algorithm 1.

Since $\mathcal{D}^t(\lambda_t, \mu_t)$ is concave, we can obtain that, for any $\tau \geq 0$ and $(\lambda_t, \mu_t) \in \mathbb{R}_+^L \times \mathbb{R}$, $\triangle_{\mathcal{D}^t}(\lambda_t, \mu_t; \xi_t^\tau, \zeta_t^\tau)$ is non-negative, i.e., $\triangle_{\mathcal{D}^t}(\lambda_t, \mu_t; \xi_t^\tau, \zeta_t^\tau) \geq 0$. Thus, the inequality (41) gives rise to

$$\begin{aligned} &\frac{\mathcal{D}^t(\lambda_t, \mu_t) - \mathcal{D}^t\left(\lambda_t^{\tau+1}, \mu_t^{\tau+1}\right)}{(\theta^\tau)^2} + \frac{L_t}{2} \|(\lambda_t, \mu_t) - \left(v_t^{\tau+1}, \omega_t^{\tau+1}\right)\|^2 \\ \leq\ &\frac{1 - \theta^\tau}{(\theta^\tau)^2} \left(\mathcal{D}^t(\lambda_t, \mu_t) - \mathcal{D}^t(\lambda_t^\tau, \mu_t^\tau) \right) + \frac{L_t}{2} \|(\lambda_t, \mu_t) - (v_t^\tau, \omega_t^\tau)\|^2, \end{aligned} \tag{42}$$

Summing over $\iota = 0, \ldots, \tau$ for the inequality (42) and using the fact that

$$\sum_{\iota=0}^{\tau} \frac{1}{\theta^\iota} = \frac{1}{(\theta^\tau)^2},$$

we have, for any $(\lambda_t, \mu_t) \in \mathbb{R}^L_+ \times \mathbb{R}$,

$$\frac{\mathcal{D}^t(\lambda_t, \mu_t) - \mathcal{D}^t\left(\lambda_t^{\tau+1}, \mu_t^{\tau+1}\right)}{(\theta^\tau)^2} + \frac{L_t}{2}\|(\lambda_t, \mu_t) - \left(\nu_t^{\tau+1}, \omega_t^{\tau+1}\right)\|^2 \le \frac{L_t}{2}\|(\lambda_t, \mu_t) - \left(\lambda_t^0, \mu_t^0\right)\|^2. \tag{43}$$

Taking $(\lambda_t, \mu_t) = (\lambda_t^*, \mu_t^*)$ in (43) and dropping the non-negative term $\frac{L_t}{2}\|(\lambda_t^*, \mu_t^*) - (\nu_t^{\tau+1}, \omega_t^{\tau+1})\|^2$, it leads to

$$\frac{\mathcal{D}^t(\lambda_t^*, \mu_t^*) - \mathcal{D}^t\left(\lambda_t^{\tau+1}, \mu_t^{\tau+1}\right)}{(\theta^\tau)^2} \le \frac{L_t}{2}\|(\lambda_t^*, \mu_t^*) - \left(\lambda_t^0, \mu_t^0\right)\|^2. \tag{44}$$

By an inductive argument, it follows from Step 13 of Algorithm 1 that $\theta^\tau \le 2/(\tau+2)$ for all $\tau \ge 0$. Thus, we have

$$\mathcal{D}^t(\lambda_t^*, \mu_t^*) - \mathcal{D}^t\left(\lambda_t^{\tau+1}, \mu_t^{\tau+1}\right) \le \frac{2L_t}{(\tau+2)^2}\|(\lambda_t^*, \mu_t^*) - \left(\lambda_t^0, \mu_t^0\right)\|^2. \tag{45}$$

By letting $C = 2L_t\|(\lambda_t^*, \mu_t^*) - (\lambda_t^0, \mu_t^0)\|^2$ in (45), the result (1) of the proposition is then obtained.

We next prove the result (2) of the proposition.

Let $\mathbf{y}_t(\lambda_t, \mu_t)$ be given by (34). From the definition of $\mathcal{L}^t(\mathbf{y}_t; \lambda_t, \mu_t)$ given by (32) and the strong convexity of $f(\mathbf{y}_t)$, we have, for any $\mathbf{y}_t$

$$\mathcal{L}^t(\mathbf{y}_t; \lambda_t, \mu_t) - \mathcal{L}^t(\mathbf{y}_t(\lambda_t, \mu_t); \lambda_t, \mu_t) \ge ||\mathbf{y}_t - \mathbf{y}_t(\lambda_t, \mu_t)||_2^2. \tag{46}$$

On the other hand, we have for any $(\lambda_t, \mu_t) \in \mathbb{R}^L_+ \times \mathbb{R}$,

$$\begin{aligned}
&\mathcal{L}^t(\mathbf{y}_t^*; \lambda_t, \mu_t) - \mathcal{L}^t(\mathbf{y}_t(\lambda_t, \mu_t); \lambda_t, \mu_t)\\
&= f(\mathbf{y}_t^*) + \lambda_t^\top \mathbf{g}(\mathbf{y}_t^*) + \mu_t h(\mathbf{y}_t^*) - \mathcal{D}^t(\lambda_t, \mu_t)\\
&= \mathcal{D}^t(\lambda_t^*, \mu_t^*) + \lambda_t^\top \mathbf{g}(\mathbf{y}_t^*) + \mu_t h(\mathbf{y}_t^*) - \mathcal{D}^t(\lambda_t, \mu_t)\\
&\le \mathcal{D}^t(\lambda_t^*, \mu_t^*) - \mathcal{D}^t(\lambda_t, \mu_t),
\end{aligned}$$

where we uses the facts that $f(\mathbf{y}_t^*) = \mathcal{D}^t(\lambda_t^*, \mu_t^*)$ due to the *strong duality* in the second equality, and $\mathbf{g}(\mathbf{y}_t^*) \preceq \mathbf{0}$ and $\lambda_t \succeq \mathbf{0}$ in the last inequality. Thus, by combined with (46), we get

$$||\mathbf{y}_t^* - \mathbf{y}_t(\lambda_t, \mu_t)||_2^2 \le \mathcal{D}^t(\lambda_t^*, \mu_t^*) - \mathcal{D}^t(\lambda_t, \mu_t), \quad \forall\ (\lambda_t, \mu_t) \in \mathbb{R}^L_+ \times \mathbb{R}.$$

Taking $(\lambda_t, \mu_t) = (\lambda_t^{\tau+1}, \mu_t^{\tau+1})$ and $\mathbf{y}_t(\lambda_t, \mu_t) = \mathbf{y}_t^{\tau+1}$ in the above inequality, and making use of the result (1) obtained, we have, for all $\tau \ge 0$,

$$||\mathbf{y}_t^* - \mathbf{y}_t^{\tau+1}||_2^2 \le \mathcal{D}^t(\lambda_t^*, \mu_t^*) - \mathcal{D}^t\left(\lambda_t^{\tau+1}, \mu_t^{\tau+1}\right) \le \frac{C}{(\tau+2)^2},$$

which proves the rest part of the proposition. □

References

[1] J. García-Villalobos, I. Zamora, J.I.S. Martín, F.J. Asensio, V. Aperribay, Plug-in electric vehicles in electric distribution networks: a review of smart charging approaches, Renew. Sustain. Energy Rev. 38 (2014) 717–731.
[2] A. Gurtu, M.Y. Jaber, C. Searcy, Impact of fuel price and emissions on inventory policies, Appl. Math. Model. 39 (3–4) (2015) 1202–1216.
[3] X. Hu, Y. Zou, Y. Yang, Greener plug-in hybrid electric vehicles incorporating renewable energy and rapid system optimization, Energy 111 (2016) 971–980.
[4] Z. Hu, K. Zhan, H. Zhang, Y. Song, Pricing mechanisms design for guiding electric vehicle charging to fill load valley, Appl. Energy 178 (2016) 155–163.
[5] X. Wu, X. Hu, S. Moura, X. Yin, V. Pickert, Stochastic control of smart home energy management with plug-in electric vehicle battery energy storage and photovoltaic array, J. Power Sources 333 (2016) 203–212.
[6] X. Hu, S.J. Moura, N. Murgovski, B. Egardt, D. Cao, Integrated optimization of battery sizing, charging, and power management in plug-in hybrid electric vehicles, IEEE Trans. Control Syst. Technol. 24 (3) (2016) 1036–1043.
[7] X. Hu, C.M. Martinez, Y. Yang, Charging, power management, and battery degradation mitigation in plug-in hybrid electric vehicles: a unified cost-optimal approach, Mech. Syst. Signal Process. 87 (2017) 4–16.
[8] Y. Cao, S. Tang, C. Li, P. Zhang, Y. Tan, Z. Zhang, J. Li, An optimized EV charging model considering TOU price and SOC curve, IEEE Trans. Smart Grid 3 (1) (2012) 388–393.
[9] H. Yang, S. Yang, Y. Xu, E. Cao, Z. Dong, M. Lai, Electric vehicle route optimization considering time-of-use electricity price by learnable partheno-genetic algorithm, IEEE Trans. Smart Grid 6 (2) (2015) 657–666.
[10] C.L. Floch, F. Belletti, S. S. Moura, Optimal charging of electric vehicles for load shaping: a dual-splitting framework with explicit convergence bounds, IEEE Trans. Transp. Electrif. 2 (2) (2016) 190–199.
[11] L. Gan, U. Topcu, S. Low, Optimal decentralized protocol for electric vehicle charging, IEEE Trans. Power Syst. 28 (2) (2013) 940–951.
[12] J. Li, C. Li, Y. Xu, Z.Y. Dong, K.P. Wong, T. Huang, Noncooperative game-based distributed charging control for plug-in electric vehicles in distribution networks, IEEE Trans. Ind. Informat. (2016), doi:10.1109/TII.2016.2632761.
[13] Z. Ma, D.S. Callaway, I.A. Hiskens, Decentralized charging control of large populations of plug-in electric vehicles, IEEE Trans. Control Syst. Technol. 21 (1) (2013) 67–78.
[14] N. Chen, C. Tan, T. Quek, Electric vehicle charging in smart grid: optimality and valley-filling algorithms, IEEE J. Sel. Topics Signal Process. 8 (6) (2014) 1073–1083.
[15] W. Tushar, W. Saad, H.V. Poor, D.B. Smith, Economics of electric vehicle charging: a game theoretic approach, IEEE Trans. Smart Grid 3 (4) (2012) 1767–1778.
[16] S. Boyd, N. Parikh, E. Chu, B. Peleato, J. Eckstein, Distributed optimization and statistical learning via the alternating direction method of multipliers, Found. Trends Mach. Learn. 3 (1) (2011) 1–122.

[17] J. Li, Z. Wu, C. Wu, Q. Long, X. Wang, An inexact dual fast gradient-projection method for separable convex optimization with linear coupled constraints, J. Optim. Theory Appl. 168 (1) (2016) 153–171.
[18] A. Javaherian, M. Soleimani, K. Moeller, A. Movafeghi, R. Faghihi, An accelerated version of alternating direction method of multipliers for TV minimization in EIT, Appl. Math. Model. 40 (21–22) (2016) 8985–9000.
[19] E. Hassannayebi, S.H. Zegordi, M. Yaghini, Train timetabling for an urban rail transit line using a lagrangian relaxation approach, Appl. Math. Model. 40 (23–24) (2016) 9892–9913.
[20] J. Liu, C. Wu, J. Cao, X. Wang, K.L. Teo, A binary differential search algorithm for the 0–1 multidimensional knapsack problem, Appl. Math. Model. 40 (23–24) (2016) 9788–9805.
[21] C. Zhao, C. Wu, J. Chai, X. Wang, X. Yang, J.M. Lee, M.J. Kim, Decomposition-based multi-objective firefly algorithm for RFID network planning with uncertainty, Appl. Soft Comput. 55 (2017) 549–564.
[22] J. Li, C. Wu, Z. Wu, Q. Long, Gradient-free method for nonsmooth distributed optimization, J. Global Optim. 61 (2) (2015) 325–340.
[23] Z. Tan, P. Yang, A. Nehorai, An optimal and distributed demand response strategy with electric vehicles in the smart grid, IEEE Trans. Smart Grid 5 (2) (2014) 861–869.
[24] J. Rivera, C. Goebel, H.A. Jacobsen, Distributed convex optimization for electric vehicle aggregators, IEEE Trans. Smart Grid (2015), doi:10.1109/TSG.2015.2509030.
[25] S. Habib, M. Kamran, U. Rashid, Impact analysis of vehicle-to-grid technology and charging strategies of electric vehicles on distribution networks-a review, J. Power Sources 277 (2015) 205–214.
[26] J. Taylor, A. Maitra, M. Alexander, D. Brooks, M. Duvall, Evaluation of the impact of plug-in electric vehicle loading on distribution system operations, Power Energy Soc. General Meet. (2009). PES'09 (pp. 1–6). IEEE
[27] A.D. Hilshey, P.D.H. Hines, P. Rezaei, J.R. Dowds, Estimating the impact of electric vehicle smart charging on distribution transformer aging, IEEE Trans. Smart Grid 4 (2) (2013) 905–913.
[28] C. Li, C. Liu, K. Deng, X. Yu, T. Huang, Data-driven charging strategy of PEVs under transformer aging risk, IEEE Trans. Control Syst. Technol. (2017), doi:10.1109/TCST.2017.2713321.
[29] E.R.M. Oz, G. Razeghi, L. Zhang, F. Jabbari, Electric vehicle charging algorithms for coordination of the grid and distribution transformer levels, Energy 113 (2016) 930–942.
[30] K. Clement-Nyns, E. Haesen, J. Driesen, The impact of charging plug-in hybrid electric vehicles on a residential distribution grid, IEEE Trans. Power Syst. 25 (1) (2010) 371–380.
[31] S. Shao, M. Pipattanasomporn, S. Rahman, Demand response as a load shaping tool in an intelligent grid with electric vehicles, IEEE Trans. Smart Grid 2 (4) (2015) 624–631.
[32] A. Ghavami, K. Kar, A. Gupta, Decentralized charging of plug-in electric vehicles with distribution feeder overload control, IEEE Trans. Autom. Control (2016), doi:10.1109/TAC.2016.2516240.
[33] A.G. Pakdehi, Price-Driven Charging of Plug-in Electric Vehicles in the Smart Grid [d], rensselaer Polytechnic institute, 2014.
[34] O. Ardakanian, S. Keshav, C. Rosenberg, Real-time distributed control for smart electric vehicle chargers: from a static to a dynamic study, IEEE Trans. Smart Grid 5 (5) (2014) 2295–2305.
[35] Z. Ma, S. Zou, X. Liu, A distributed charging coordination for large-scale plug-in electric vehicles considering battery degradation cost, IEEE Trans. Control Syst. Technol. 23 (5) (2015) 2044–2052.
[36] J. Zhang, Y. Wei, H. Qi, State of charge estimation of lifePO4 batteries based on online parameter identification, Appl. Math. Model. 40 (11–12) (2016) 6040–6050.
[37] B. Ramanathan, V. Vittal, A framework for evaluation of advanced direct load control with minimum disruption, IEEE Trans. Power Syst. 23 (4) (2008) 1681–1688.
[38] C. Li, X. Yu, W. Yu, G. Chen, J. Wang, Efficient computation for sparse load shifting in demand side management, IEEE Trans. Smart Grid (2016), doi:10.1109/TSG.2016.2521377.
[39] F. Dörfler, M.R. Jovanović, M. Chertkov, F. Bullo, Sparsity-promoting optimal wide-area control of power networks, IEEE Trans Power Syst. 29 (5) (2014) 2281–2291.
[40] D.T. Phan, A.S. Xu, Minimal impact corrective actions in security-constrained optimal power flow via sparsity regularization, IEEE Trans. Power Syst. 30 (4) (2015) 1947–1956.
[41] C.K. Wen, J.C. Chen, J.H. Teng, P. Ting, Decentralized plug-in electric vehicle charging selection algorithm in power systems, IEEE Trans. Smart Grid 3 (4) (2012) 1779–1789.
[42] J. Li, G. Chen, Z.Y. Dong, Z. Wu, A fast dual proximal-gradient method for separable convex optimization with linear coupled constraints, Comput. Optim. Appl. 64 (3) (2016) 671–697.
[43] W.H. Kersting, Radial distribution test feeders, in: IEEE Power Engineering Society Winter Meeting, Columbus, OH, 2011, pp. 908–912.
[44] Y.M. Atwa, E.F. El-Saadany, Optimal allocation of ESS in distribution systems with a high penetration of wind energy, IEEE Trans. Power Syst. 25 (4) (2010) 1815–1822.